Published in final edited form as:
NMR Biomed. 2014 March ; 27(3): 332–340. doi:10.1002/nbm.3067.

Quantitative assessment of global cerebral metabolic rate of oxygen ($CMRO_2$) in neonates using MRI

Peiying Liu[a], **Hao Huang**[a,b], **Nancy Rollins**[b,d], **Lina F. Chalak**[c], **Tina Jeon**[a], **Cathy Halovanic**[d], and **Hanzhang Lu**[a,b]

[a]Advanced Imaging Research Center, University of Texas Southwestern Medical Center, Texas, United States

[b]Department of Radiology, University of Texas Southwestern Medical Center, Dallas, Texas, United States

[c]Department of Pediatrics, University of Texas Southwestern Medical Center, Dallas, Texas, United States

[d]Children's Medical Center of Dallas, Dallas, Texas, United States

Abstract

Cerebral metabolic rate of oxygen ($CMRO_2$) is the rate of oxygen consumption by the brain and is thought to be a direct index of energy homeostasis and brain health. However, *in vivo* measurement of $CMRO_2$ has been challenging, in particular for neonatal population in whom conventional radiotracer methods are not applicable due to safety concerns. In this study, we propose a method to quantify global $CMRO_2$ in neonates based on arteriovenous differences in oxygen content and employ separate measurements of oxygenation and CBF parameters. Specifically, arterial and venous oxygenation levels were determined with pulse oximetry and a novel T_2-Relaxation-Under-Spin-Tagging (TRUST) MRI, respectively. Global CBF was measured with a phase-contrast (PC) flow velocity MRI. The proposed method was implemented on a standard 3T MRI without the need of any exogenous tracers and the total scan duration was less than 5 minutes. We demonstrated the feasibility of this method in twelve healthy neonates within an age range of 35–42 gestational weeks. $CMRO_2$ values were successfully obtained from ten neonates. It was found that average $CMRO_2$ in this age range was 38.3±17.7 μmol/100g/min and was positively correlated with age (p=0.007, slope 5.2 μmol/100g/min per week), although the highest $CMRO_2$ value in this age range was still less than half of the adult level. Test-retest studies showed a coefficient of variation of 5.8±2.2 % between repeated $CMRO_2$ measurements. Additionally, given the highly variable blood flow velocity within this age range, it is recommended that the TRUST labeling thickness and position should be determined on a subject-by-subject basis, and an automatic algorithm was developed for this purpose. Although this method provides a global $CMRO_2$ measure only, the clinical significance of an energy consumption marker and the convenience of this technique may make it a useful tool in functional assessment of neonatal population.

Keywords

$CMRO_2$; brain; fetus; baby; TRUST; energy consumption

Corresponding Author: Peiying Liu or Hanzhang Lu, Advanced Imaging Research Center, UT Southwestern Medical Center, 5323 Harry Hines Blvd., Dallas, TX 75390, peiying.liu@utsouthwestern.edu or hanzhang.lu@utsouthwestern.edu, Tel: 214-645-2806, Fax: 214-645-2744.

Introduction

Cerebral oxidative metabolism plays a critical role in the early development of the brain. Starting from the third trimester and continuing several months after birth, the form of energy production in the human brain shifts from anaerobic glycolysis to the more energy-efficient aerobic metabolism, in order to meet the escalating cerebral energy demands during rapid structural and functional development (1). Therefore, disruption of oxygen supply and metabolism at this stage is particularly detrimental, and has been associated with several cerebral injuries, such as hypoxic-ischemic encephalopathy, stroke, and metabolic disorders, all of which may lead to long-term neurologic deficits (2–4). As a result, quantitative assessment of cerebral oxygen metabolism in the neonate is important for better understanding normal brain development and the etiology of various neonatal brain injuries, as well as for the diagnosis and treatment assessment of these injuries on an individual basis.

There exist considerable challenges in the measurement of cerebral oxygen metabolism in neonates. Positron Emission Tomography (PET) is the gold standard for the measurement of cerebral metabolic rate of oxygen ($CMRO_2$) in adults (5), but its applicability in neonates is limited by the concerns of radiation safety in this population. Near infrared spectroscopy (NIRS) approaches have been proposed to assess $CMRO_2$ (6–10), but have not been widely accepted because assumptions on arteriovenous volume ratio are required, and it is difficult to determine the light penetration depth. Other potential $CMRO_2$ methods, such as the ^{13}C NMR (11), ^{17}O NMR (12), and biophysical model based MRI methods (13–15), have only begun to be explored in adults and are not ready to be used in neonates. As a result of these technical obstacles, little is known about the brain's metabolic rate in neonates, and normal values of $CMRO_2$ in human neonates are not well established.

The purpose of the present study is to develop a global $CMRO_2$ method that is rapid (<5 minutes), quantitative (in physiologic units), and can be performed on a standard 3T MRI system. This method is based on arteriovenous differences in oxygen content and does not require any exogenous tracers. Feasibility of the proposed method is demonstrated in 12 healthy neonatal subjects with an age range of 35 to 42 gestational weeks. Intra-session test-retest reproducibility is also evaluated. $CMRO_2$ values are reported for 10 of the participants examined in this study.

Materials and Methods

Framework of $CMRO_2$ quantification

The framework of our $CMRO_2$ measurement is based on the Fick Principle (Figure 1a), in which global $CMRO_2$ can be quantified from arteriovenous differences in oxygen content (16):

$$CMRO_2 = CBF \cdot (Y_a - Y_v) \cdot C_a. \quad [1]$$

where CBF is global cerebral blood flow, Y_a and Y_v are oxygen saturation fraction in arterial and venous blood, respectively, and C_a is a constant representing the capacity of blood to carry O_2 and is well established in physiology literature (0.204 μmol O_2/ml blood per hematocrit unit (17)). Thus, once Y_a, Y_v and CBF are experimentally determined, $CMRO_2$ in units of μmol O_2/100 g/min can be calculated.

In Equation [1], global CBF can be measured by phase-contrast (PC) MRI performed at the feeding arteries of the brain, which are the left and right internal carotid arteries, and left and right vertebral arteries. PC MRI utilizes the phase of an image to encode the velocity of moving spins and has been validated for angiogram and quantitative flow measurements

(18–20). Y_a can be obtained using pulse oximetry with the optical sensor attached to the toe of the neonates, which is continuously monitored in neonatal scans. The most challenging component, venous oxygenation (Y_v), is measured by a T_2-relaxation-under-spin-tagging (TRUST) MRI technique that has recently been developed and validated in our laboratory (21–23). TRUST MRI utilizes the spin-tagging principle on the venous side to separate the pure venous blood signal from the surrounding tissue signal by subtracting a labeled image from a control image. The venous blood signal is then modulated with different T_2 weightings using various numbers of flow-insensitive T_2-preparation pulses. The mono-exponential fitting of the blood signal to the T_2-preparation duration (termed effective echo time [eTE]) gives the T_2 value of the venous blood, which is further converted to Y_v via the relationship between blood T_2 and oxygenation (22,24). TRUST MRI technique has been optimized (23,25) and validated in adults against a gold-standard pulse oximetry method (22), but has not been performed in neonates previously.

Participants

Twelve healthy neonates (8 males and 4 females) were recruited from the Perinatal-Neonatal Clinic in the Parkland Memorial Hospital. The sample was drawn from an ongoing research project at the University of Texas Southwestern Medical Center (UTSW) to study prenatal and perinatal human brain development with MRI. The study protocol was approved by the UTSW Institutional Review Board of the UTSW. Parents of the neonates gave informed written consent before participating in the study. The mean and standard deviation of gestational age of recruited neonates at birth was 34.5±4.8 weeks, ranging from 28.9 to 41.3 weeks. The mean and standard deviation of gestational age of recruited neonates at the time of the study was 37.4± 2.6 weeks, ranging from 34.7 to 41.6 weeks. The recruited neonates had no neurological event at birth, no presence of known or suspected congenital anomalies such as chromosomal anomalies, no major congenital heart disease or congenital infection, and no substance abuse. The neonates were also excluded for a grade>1 on intraventricular hemorrhage (IVH), and the presence of cystic periventricular leukomalacia (PVL), both measured by cranial ultrasound. None of the neonates required respiratory support at the time of study.

General MRI data acquisition

All MRI scans were performed on a 3T MRI system (Philips Medical Systems, Best, the Netherlands) using a body coil for transmission and an eight-channel phased-array coil for reception. No sedation was used. The neonates were well fed before MRI scan and wrapped with a vacuum immobilizer to minimize motion.

The MRI session began with a series of clinical sequences including T_2 and FLAIR. A pediatric neuroradiologist read the images to confirm the absence of radiographic abnormalities.

The protocol for a complete set of $CMRO_2$ data is shown in Figure 1b. Measurement of Y_v requires two scans, a localizer PC MRI and a TRUST MRI. Measurement of CBF requires five scans, an angiogram and four quantitative PC MRI. The details of these scans are described in the following two sub-sections.

MRI scans to measure Y_v

A localizer PC MRI scan was performed with the imaging slab centered at the mid-sagittal plane to provide a quantitative map of venous flow velocity along the entire path of the superior sagittal sinus (Figure 2a). This information was used to determine the optimal labeling position for the TRUST MRI sequence. The imaging parameters of the localizer PC

MRI were: FOV=130 × 130 × 8 mm^3, voxel size=0.6 × 0.8 × 2 mm^3, TR=20ms, V_{enc}=15 cm/s, flow encoding in three orthogonal directions in separate TRs, scan duration = 54 s.

The imaging slice of TRUST MRI was positioned to be parallel to anterior-commissure posterior-commissure line with a distance of 15 mm from the sinus confluence where the superior sagittal sinus (SSS), straight sinus and transverse sinus join (Figure 2a). The distance value of 15 mm was chosen empirically for protocol standardization purposes and was shorter than the value (20 mm) used for adult TRUST MRI protocol (25). This criterion allowed the imaging slice to intersect SSS at an angle close to 90°. Note that the imaging slice is not required to be perfectly perpendicular to the SSS since the spin-tagging principle utilized in TRUST separates the venous blood from static tissue with minimal partial voluming effect. Details of the TRUST pulse sequence has been described extensively in the literature (21,23). In this study, a postsat TRUST sequence (23) was used. Imaging parameters for the neonatal TRUST MRI scan were modified from the adult scan parameters (23,25) to account for the smaller brain size in the neonates. The neonate scan used the following values: TR = 3000 ms, TI = 1022 ms, FOV = 120 × 120 × 5 mm^3, matrix size = 64 × 56, SENSE factor = 3, voxel size = 1.88 × 2.14 × 5 mm^3, four different T_2-weightings with eTEs of 0 ms, 40 ms, 80 ms and 160 ms, with a τ_{CPMG} = 10 ms, 3 pairs of control and label images for each eTE, scan duration = 72 s.

Since TRUST MRI uses the spin-tagging principle to separate pure venous blood from tissue, effective labeling of the blood is important to obtain high quality results. In the TRUST sequence, a labeling slab is placed above the imaging plane, so that at the time of acquisition, the blood in the imaging slice has previously experienced the inversion pulse (21). In adults, this requirement can be met effectively in virtually all subjects with a fixed setting of 100 mm thick labeling slab, and a 22.5 mm gap between the labeling slab and the imaging plane(25). However, due to rapid brain development in neonates, blood flow velocity could vary by up to 3 fold across individuals. Thus, an individual-specific labeling parameter set (including labeling slab thickness and labeling gap) may be preferable over a fixed labeling scheme. Therefore, an automatic algorithm was developed to determine the TRUST MRI labeling parameters during the scan session from the localizer PC MRI scan described above.

The gist of the algorithm is to determine where the imaged blood spins are originating from. The spatial location of the blood spins at the time 1022 ms (i.e. the post-labeling delay TI) prior to arriving at the imaging plane, i.e. at the time right after the labeling pulse, is somewhere upstream in the SSS. Once this point of origin is found, it will determine the placement of the center of the labeling slab. The inputs to the algorithm are the velocity map of the SSS obtained from the localizer PC MRI scan (Figure 2a) and the coordinates of the imaging location on the SSS (filled circle in Figure 2a). The algorithm first identifies the trajectory of the SSS based on the highest flow velocity in the upwards neighboring voxels. Next, the time required to traverse adjacent voxels on the trajectory was calculated. Then, the location of the blood at 1022 ms prior to reaching the imaging slice is determined, which is set to be the center of labeling slab. Finally, the thickness of the labeling slab and the gap between labeling slab and imaging plane are determined, such that the gap is 10% of the labeling thickness. This gap is used to minimize direct saturation effect from the labeling RF pulse on the imaging slice.

To evaluate the efficacy of this automatic algorithm, in five neonates, we compared the TRUST MRI results between the automatic method and a method using a fixed parameter set. The fixed parameter set used a labeling thickness of 60 mm and a gap of 6 mm.

MRI scans to measure CBF

First, a Time-Of-Flight angiogram was performed with axial slices encompassing a slab covering foramen magnum (Figure 3a). The resulting images allowed visualization of the feeding arteries (Figure 3b) and were used for the positioning of the arterial PC MRI scans. The imaging parameters of the angiogram were: TR/TE/flip angle = 20 ms/3.45 ms/18°, FOV = 100 × 100 × 20 mm^3, voxel size = 1.0 × 1.0 × 2 mm^3, one 60 mm saturation slab positioned above the imaging slab, scan duration = 19 s.

The planning of the four quantitative PC MRI scans was based on the maximum-intensity-projection (MIP) images from the angiogram. Each scan was planned on one of the four feeding arteries of the brain, left internal carotid artery (left ICA), right internal carotid artery (right ICA), left vertebral artery (left VA) and right vertebral artery (right VA) (Figure 3b). The slices for the left and right ICAs were positioned at the level of foramen magnum where the arteries enter the skull. However, the placement of the imaging plane for the VAs requires more care, since the VAs have a complex anatomy at the neck region. These arteries are known to make two turns within their V3 segment, one below and the other above the C1 vertebral column (26). Thus, we chose to place the imaging slice between the two turns in V3 segments, at approximately the level of C1 vertebral column. Imaging parameters of PC MRI were: single slice, voxel size = 0.6 × 0.8 × 3 mm^3, FOV = 120 × 120 × 3 mm^3, maximum velocity encoding = 10 cm/s, non-gated, 4 averages, scan duration of each artery is 24s.

With the above protocol, the total duration to obtain a neonatal $CMRO_2$ dataset is approximately 4.1 minutes. In three subjects, the $CMRO_2$ protocol was repeated once without repositioning to provide an assessment of intra-session test-retest reproducibility of the results.

Data analysis

Data processing of TRUST MRI and arterial PC MRI followed methods described previously (25,27). Briefly, the TRUST MRI data was motion corrected using the software Statistical Parametric Mapping (SPM2, University College London, UK). Then a pairwise subtraction between control and labeled images results in pure blood signal, on which a preliminary region-of-interest (ROI) was manually drawn to include the superior sagittal sinus. The six voxels with the largest signal intensity were chosen within the ROI for spatial averaging. The averaged venous blood signal for each eTE was then fit to a mono-exponential model to obtain a blood T_2. A goodness-of-fit index, ΔR_2 (where $R_2=1/T_2$), was also computed in the fitting procedure, which is defined as the 95% confidence interval of R_2. ΔR_2 is a measure of the estimation uncertainty (95% confidence interval) of the mono-exponential fitting. Smaller ΔR_2 indicates better precision of the T_2 quantification. The T_2 was in turn converted to Y_v via a calibration plot established by in vitro blood experiments using subject-specific hematocrit values. For PC MRI data, each PC MRI scan generated three images, an anatomic image, a magnitude image and a velocity map. A ROI was manually drawn on the magnitude image of the target artery from each PC MRI scan. The operator was instructed to trace the boundary of only the target artery based on the intensity difference between the vessel region and background tissue. The ROI drawn on the magnitude image was then applied to the velocity map. The velocity values from individual voxels within the ROI were summed to yield the total blood flow of each artery. To account for brain size differences, the unit volume CBF (in ml/100 g/min) was obtained by normalizing the total CBF (in ml/min) of all four arteries to brain parenchyma volume, which was estimated from the clinical T_2 image (resolution 0.4 × 0.4 × 3.5 mm^3, 27 slices) using the software FSL (FMRIB Software Library, Oxford University). To estimate the brain parenchyma volume, manual skull-stripping was done in 3D slicer (28), and then the

FAST tool in FSL was used to segment the T2 image of the brain into gray matter, white matter, and CSF. The brain's parenchyma volume was given by the sum of gray and white matter volumes, and then converted to the weight of the brain by assuming a parenchyma density of 1.06 g/ml (29).

As the blood flow quantification involves manual ROI selection, inter-rater reliability was evaluated by having two raters (PL and HL) analyze the same datasets independently and calculating the correlation of the blood flow values.

Statistical analysis

Linear regression between the gestational age at the time of the scan and $CMRO_2$ was performed to evaluate the brain metabolic changes in the first few weeks of life. Comparison between TRUST MRI results using fixed labeling parameters and subject-specific parameters was conducted using paired Student t-test. A p value < 0.05 was considered statistically significant.

Results

Data from two neonates (2 males. 35 weeks and 39 weeks of gestational age at the time of the scan) were not usable due to excessive motion artifacts. Thus, the results are reported from 10 remaining subjects. Figure 2b shows representative images of neonatal TRUST MRI. It can be seen that the control and label images are visually similar, but the subtraction clearly highlights the vessel signals. Note that the images have a low resolution (1.88×2.14 mm^2) because of the use of single-shot Echo-Planar-Imaging (EPI) acquisition. However, we point out that partial volume between blood and tissue is accounted for by the TRUST subtraction scheme, thus the difference signal contains only pure blood. One can also see a fat artifact in the image. This is expected because fat saturation was not employed in the sequence in order to minimize the time gap between the tip-up of the T_2-preparation and the excitation RF pulse. This fat artifact does not overlap with our area of interest (i.e. SSS), and does not negatively impact the quality of our data. With increasing eTE, image intensities in the control, labeled, and difference images all show attenuation. The difference signal in the SSS is plotted as a function of eTE in Figure 2c. The resulting blood T_2 and the estimated Y_v are also shown in the figure. The average Y_v value of this neonatal cohort was 63.9±8.2% (mean±SD, N=10). Interestingly, these values are similar to the adult Y_v of 64.8±6.3% (21). The goodness-of-fit index, ΔR_2, was found to be 4.62 ±2.46. This range is larger than the adult values of 2.44 ±1.10 (30). Y_a in this cohort was 95.8±2.2%.

Figure 3b shows representative images of the angiogram (middle) and PC MRI velocity maps of the feeding arteries (corners). The average CBF value in the neonates was 14.9±4.9 ml/100g/min. In contrast to Y_v, neonatal CBF values were considerably lower than the adult values of 60.6±9.7 ml/100g/min (25) using similar measurement techniques. Note that these CBF values have been normalized to per unit mass, thus are not attributable to the smaller brain volume in neonates. For CBF processing which involves manual ROI drawing, we observed a high inter-rater reliability of $r = 0.98$ and $P < 0.0001$.

$CMRO_2$ as calculated from the measured CBF, Y_v, and Y_a was 38.3±17.7 μmol/100g/min. Linear regression analysis showed a significant positive relationship between the gestational age of the neonates at the time of the scan and the measured $CMRO_2$ ($r = 0.78$, $p = 0.007$), as shown in Figure 4. Thus, a considerable portion of the intersubject variation in estimated $CMRO_2$ appears to be of physiologic origin and can be attributed to age-related alterations in brain metabolic rate. For reference, adult $CMRO_2$ has been shown to be in the range of 150–200 μmol/100g/min (31).

Results of test-retest assessment in 3 subjects are shown in Figure 5. The coefficient of variation (CoV), defined as standard deviation divided by mean across repetitions, of Y_v, CBF, and $CMRO_2$ were 2.54 ±1.54 %, 6.89±4.38 % and 5.78±2.17 %, respectively. The CoV of Y_v is similar to that in adults (1.88% (25)). But the CoV values of CBF and $CMRO_2$ were considerably higher than those in adults (2.77% for CBF and 3.84% for $CMRO_2$ (25)). Since CoV is a ratio term, this can be partly attributed to the lower physiologic values (i.e. smaller denominator in the CoV calculation) of these parameters in neonates. For standard deviation across repetitions, it consists of both physiological and thermal noise. The thermal noise does not scale with the mean value, thus the numerator in the CoV calculation is expected to be relatively constant. Therefore, the higher CoV in neonates can be explained by a lower mean value in the face of constant standard deviation.

The proposed automatic algorithm to determine the subject-specific labeling parameter set revealed that the average travel distance from the time of labeling to acquisition was 48.6±12.4 mm. This resulted in an optimal labeling thickness and gap of 57.2±13.8 mm and 5.7±1.4 mm, respectively. The 95% confidence interval of ΔR_2 using subject-specific labeling parameters (4.0±0.8 s^{-1}) was significantly smaller ($p = 0.028$, N=5) than that using fixed parameter set (6.8±2.4 s^{-1}), suggesting an improved estimation precision using the automatic algorithm. However, the estimated blood T_2 values were not different between the two types of TRUST MRI data ($p = 0.30$, N=5), indicating that there is no systematic bias between the two methods.

Discussion

We have proposed a method to quantify global $CMRO_2$ in human neonates without the use of exogenous tracers. We have demonstrated the feasibility of this method in subjects within an age range of 35–42 gestational weeks. It was further found that $CMRO_2$ has a significant dependence on age in this cohort. Test-retest studies showed reproducible $CMRO_2$ results using the proposed approach. Additionally, given the highly variable blood flow velocity within this age range, it is recommended that the labeling thickness and position should be determined on a subject-by-subject basis, and we have developed an automatic algorithm for this purpose.

Although there is no previous literature on neonatal $CMRO_2$ measurement using MRI, a total of four previous reports using other imaging modalities (1 using PET and 3 using NIRS) have quantified absolute $CMRO_2$ values in neonates (8–10,32). Findings from these studies are summarized in Table 1. The first absolute $CMRO_2$ measurement in neonates was reported by Skov et al. in 1993 (9). Using NIRS combined with ^{133}Xe injection and head tilting, the investigators reported a mean $CMRO_2$ of 44.7±17.9 μmol/100g/min from 9 preterm neonates with respiratory distress syndrome and a mean $CMRO_2$ of 62.6±35.8 μmol/100g/min from 10 asphyxiated, term neonates, with a 59% success rate using their technique. In the same year, Altman et al. used PET and measured $CMRO_2$ in 10 sick newborns (32). They reported $CMRO_2$ of 2.7 to 24.1 μmol/100g/min from five preterm neonates and 17.9 to 58.1 μmol/100g/min for five termed neonates. Using NIRS with partial jugular venous occlusion, Yoxall et al. reported $CMRO_2$ values of 23.2 to 78.7 μmol/100g/min from 20 neonates under intensive care aged between 24 and 41 gestational weeks, with 8 neonates under sedation during measurement, and 3 taking medication for seizure treatment (10). More recently, Elwell et al. proposed a model based NIRS method and reported $CMRO_2$ of 30.8 to 68.4 μmol/100g/min from 9 sick neonates between 23 to 37 gestational weeks (8). The $CMRO_2$ values we observed (38.3±17.7 μmol/100g/min) are in general agreement with this scarce and highly variable literature. A difference between the present study and the previous reports is that this study used healthy neonates only, whereas the other reports were conducted on a variety of diseased populations. Thus, the values

reported in the present study may be a better representation of reference $CMRO_2$ values in healthy neonates.

An important technical advantage of the proposed method is that it is clinically practical. Therefore, once optimized, this technique can be readily translated to patient studies. Compared to prior studies that used exogenous tracers and/or required the compression of cerebral veins (9,10,32), the present method is completely non-invasive and can be performed on a standard 3T MRI. The scan duration of less than 5 minutes is also practical for most neonatal subjects.

Neonatal $CMRO_2$ values obtained in the present study, as well as in prior studies (8–10,32), showed that the brain metabolic rate is much lower in neonates compared to adults, which are typically 150–200 μmol/100g/min (31). Since these $CMRO_2$ values have been normalized to per unit mass, they are not attributable to the smaller brain volume in neonates. Furthermore, it is also interesting to note that this $CMRO_2$ variability is primarily attributed to CBF difference, but not oxygenation. Specifically, neonates have Y_v and Y_a values similar to those in adults, but their CBF value is much lower. Thus, Y_v of ~60% seems to be a critical target value for tissue function and the brain seems to have a system to adjust its blood supply to meet this target regardless the age. This indicates that the cerebral metabolism and blood supply is well coupled. Our data also suggests that the increase in $CMRO_2$ from neonate to adult values is not linear. This is evidenced by our data that a significant age-dependence can already be observed within a narrow age range of 35–42 gestational weeks. The rate of $CMRO_2$ change according to our data is 5.2 μmol/100g/min per week. Assuming that this trend continues in the following few months, it is estimated that an infant of 6 months old may already approach the adult $CMRO_2$ level.

The reason that neonatal $CMRO_2$ values are smaller than adult values may be due to lower energy demands during the neonatal period. Although there is an escalating cerebral energy demand in the third trimester (i.e., 28 weeks to delivery), the energy required by the neonatal brain is still much lower than that required by the adult brain. Previous studies have shown that the nerve cell density is much higher in the neonate than in adults (33,34), but the neonate brain has also been found to have less neuronal processes, synapses, myelination, neurotransmitters and receptors (35–37). This would lead to fewer neuronal activities in the neonate brain. In the adult brain, the majority of the oxygen delivered is consumed for neuronal activity to maintain and restore the neuronal ionic gradients required for synaptic and neural activation (38). In neonates, the electrocortical activity is also associated with concurrent changes in cerebral oxygenation (39). Therefore, less oxygen consumption is required by the neonatal brain to meet its energy demands compared to an adult brain.

The main source of error in our measurement was subject motion. As stated earlier, no sedation was used in our scan session. Thus, the approaches to minimize motion relied on sufficient feeding the neonate prior to the scan, waiting for the subject to fall asleep, and by using the vacuum immobilizer. This was not always sufficient, which resulted in the data from two subjects to be deemed unusable. The remaining 10 subjects were included in the quantitative analysis, but it should be noted that certain amount of motion was still present in these data sets. This factor may have contributed to the greater CoV observed in the neonatal data compared to adult $CMRO_2$ data.

This initial report should be viewed as a proof-of-principle study only, and further development of several technical aspects should be conducted before it can become a standard tool. First, the conversion of blood T_2 to blood oxygenation requires a calibration plot that specifies the relationship between these two parameters. At present, the calibration plot used in our study is based on data from adult blood samples (22). However, the human

neonate is known to have an additional type of hemoglobin called fetal hemoglobin, which has a slightly different molecular structure (thus oxygen affinity) compared to the adult form (40). Although no studies have shown this, it is possible that the T_2 value of the neonatal blood is different from that of the adult blood, even at identical oxygen saturation and hematocrit levels. Therefore, future studies are needed to establish a calibration plot based specifically on neonatal blood, and to examine whether a difference exists in the T_2 relaxometry of neonatal and adult blood. Another limitation of the present study is that the venous oxygenation was based on measurement in the superior sagittal sinus above the location of sinus confluence. While SSS is a major draining vein and its oxygenation can be considered as a global value averaged over the cortical areas, subcortical regions are drained by another vein called the straight sinus, which was not included in the SSS measurement. Thus, future work should aim to measure both SSS and straight sinus simultaneously in a single scan, which could be possible by tilting the image slice to intersect both vessels. Moreover, the intra-session test-retest reproducibility evaluated in this study only examined the measurement errors caused by physiological variation and instrument noise. Therefore, more comprehensive evaluation should be performed in the future to assess the repositioning error and scan operator dependence. Finally, the proposed technique provides a global measure only but lacks spatial information. Region-specific measurement of CBF can be achieved with several non-invasive techniques, such as Arterial-Spin-Labeling (ASL) MRI (41–44). However, techniques to map venous oxygenation in the brain are still underdeveloped, especially for the neonatal population. Therefore, future technical development should focus on this direction. In the meanwhile, given the importance of the $CMRO_2$ marker and the convenience of the proposed method, the present global technique may be a useful tool to assess brain function in the neonatal population.

Conclusions

The present study demonstrated the feasibility to quantify global $CMRO_2$ in neonates using the Fick principle, with separate measurements of blood oxygenation and CBF parameters. It was shown that this method can be performed on a standard 3T MRI in less than 5 minutes without the need of any exogenous tracers. $CMRO_2$ values were obtained from 10 neonates within an age range of 35–42 gestational weeks. It was found that $CMRO_2$ increases rapidly during this period of life, although the highest value was still less than half of the adult level.

Supplementary Material

Refer to Web version on PubMed Central for supplementary material.

Acknowledgments

Grant sponsors: NIH R01 MH092535 (to HH), MH092535-S1 (to HH), NIH R01 MH084021 (to HL), NIH R01 NS067015 (to HL), NIH R01 AG042753 (to HL), and K23HD069521-01A11 (to LC).

The authors are grateful to Jared Mosher for assistance with the MRI experiments and to the nurses of the transporting team in Division of Perinatal-Neonatal Medicine in Parkland Memorial Hospital. The authors are also grateful to Lisa Krishnamurthy for scientific editing of the manuscript.

Abbreviations used

$CMRO_2$	cerebral metabolic rate of oxygen
TRUST	T_2-Relaxation-Under-Spin-Tagging

CBF	cerebral blood flow
PC	phase-contrast
PET	positron emission tomography
NIRS	near infrared spectroscopy
eTE	effective echo time
IVH	intraventricular hemorrhage
PVL	periventricular leukomalacia
FOV	field of view
TR	time of repetition
TE	echo time
TI	time of inversion
SSS	superior sagittal sinus
MIP	maximum-intensity-projection
ICA	internal carotid artery
VA	vertebral artery
ROI	region-of-interest
SD	standard deviation
CoV	coefficient of variation
ASL	Arterial-Spin-Labeling
RDS	respiratory distress syndrome
HIE	hypoxic-ischemic encephalopathy

References

1. du Plessis AJ. Cerebral blood flow and metabolism in the developing fetus. Clin Perinatol. 2009; 36(3):531–548. [PubMed: 19732612]
2. Kiechl-Kohlendorfer U, Ralser E, Pupp Peglow U, Reiter G, Trawoger R. Adverse neurodevelopmental outcome in preterm infants: risk factor profiles for different gestational ages. Acta paediatrica. 2009; 98(5):792–796. [PubMed: 19191762]
3. Trescher WH, Lehman RA, Vannucci RC. The influence of growth retardation on perinatal hypoxic-ischemic brain damage. Early human development. 1990; 21(3):165–173. [PubMed: 2311553]
4. Pape, KE.; Wigglesworth, JS. Clinics in Developmental Medicine. Mac Keith Press; 1993. Haemorrhage, Ischaemia and the Perinatal Brain; p. 1-196.
5. Mintun MA, Raichle ME, Martin WR, Herscovitch P. Brain oxygen utilization measured with O-15 radiotracers and positron emission tomography. J Nucl Med. 1984; 25(2):177–187. [PubMed: 6610032]
6. Brown DW, Hadway J, Lee TY. Near-infrared spectroscopy measurement of oxygen extraction fraction and cerebral metabolic rate of oxygen in newborn piglets. Pediatr Res. 2003; 54(6):861–867. [PubMed: 12930911]
7. Tichauer KM, Elliott JT, Hadway JA, Lee DS, Lee TY, St Lawrence K. Using near-infrared spectroscopy to measure cerebral metabolic rate of oxygen under multiple levels of arterial oxygenation in piglets. J Appl Physiol. 2010; 109(3):878–885. [PubMed: 20616228]

8. Elwell CE, Henty JR, Leung TS, Austin T, Meek JH, Delpy DT, Wyatt JS. Measurement of CMRO2 in neonates undergoing intensive care using near infrared spectroscopy. Adv Exp Med Biol. 2005; 566:263–268. [PubMed: 16594161]
9. Skov L, Pryds O, Greisen G, Lou H. Estimation of cerebral venous saturation in newborn infants by near infrared spectroscopy. Pediatr Res. 1993; 33(1):52–55. [PubMed: 8433861]
10. Yoxall CW, Weindling AM. Measurement of cerebral oxygen consumption in the human neonate using near infrared spectroscopy: cerebral oxygen consumption increases with advancing gestational age. Pediatr Res. 1998; 44(3):283–290. [PubMed: 9727702]
11. Hyder F, Chase JR, Behar KL, Mason GF, Siddeek M, Rothman DL, Shulman RG. Increased tricarboxylic acid cycle flux in rat brain during forepaw stimulation detected with 1H[13C]NMR. Proc Natl Acad Sci U S A. 1996; 93(15):7612–7617. [PubMed: 8755523]
12. Zhu XH, Zhang Y, Tian RX, Lei H, Zhang N, Zhang X, Merkle H, Ugurbil K, Chen W. Development of (17)O NMR approach for fast imaging of cerebral metabolic rate of oxygen in rat brain at high field. Proc Natl Acad Sci U S A. 2002; 99(20):13194–13199. [PubMed: 12242341]
13. An H, Lin W, Celik A, Lee YZ. Quantitative measurements of cerebral metabolic rate of oxygen utilization using MRI: a volunteer study. NMR Biomed. 2001; 14(7–8):441–447. [PubMed: 11746936]
14. Gauthier CJ, Hoge RD. Magnetic resonance imaging of resting OEF and CMRO(2) using a generalized calibration model for hypercapnia and hyperoxia. Neuroimage. 2012; 60(2):1212–1225. [PubMed: 22227047]
15. He X, Yablonskiy DA. Quantitative BOLD: mapping of human cerebral deoxygenated blood volume and oxygen extraction fraction: default state. Magn Reson Med. 2007; 57(1):115–126. [PubMed: 17191227]
16. Kety SS, Schmidt CF. The Effects of Altered Arterial Tensions of Carbon Dioxide and Oxygen on Cerebral Blood Flow and Cerebral Oxygen Consumption of Normal Young Men. J Clin Invest. 1948; 27(4):484–492. [PubMed: 16695569]
17. Guyton, AC.; Hall, JE. Respiration. In: Guyton, AC.; Hall, JE., editors. Textbook of medical physiology. Saunders/Elsevier; Philadelphia: 2005.
18. Bakker CJ, Hoogeveen RM, Viergever MA. Construction of a protocol for measuring blood flow by two-dimensional phase-contrast MRA. J Magn Reson Imaging. 1999; 9(1):119–127. [PubMed: 10030659]
19. Evans AJ, Iwai F, Grist TA, Sostman HD, Hedlund LW, Spritzer CE, Negro-Vilar R, Beam CA, Pelc NJ. Magnetic resonance imaging of blood flow with a phase subtraction technique. In vitro and in vivo validation. Invest Radiol. 1993; 28(2):109–115. [PubMed: 8444566]
20. Zananiri FV, Jackson PC, Goddard PR, Davies ER, Wells PN. An evaluation of the accuracy of flow measurements using magnetic resonance imaging (MRI). J Med Eng Technol. 1991; 15(4–5): 170–176. [PubMed: 1800748]
21. Lu H, Ge Y. Quantitative evaluation of oxygenation in venous vessels using T2-Relaxation-Under-Spin-Tagging MRI. Magn Reson Med. 2008; 60(2):357–363. [PubMed: 18666116]
22. Lu H, Xu F, Grgac K, Liu P, Qin Q, van Zijl P. Calibration and validation of TRUST MRI for the estimation of cerebral blood oxygenation. Magn Reson Med. 2012; 67(1):42–49. [PubMed: 21590721]
23. Xu F, Uh J, Liu P, Lu H. On improving the speed and reliability of T2-relaxation-under-spin-tagging (TRUST) MRI. Magn Reson Med. 2012; 68(1):198–204. [PubMed: 22127845]
24. Golay X, Silvennoinen MJ, Zhou J, Clingman CS, Kauppinen RA, Pekar JJ, van Zij PC. Measurement of tissue oxygen extraction ratios from venous blood T(2): increased precision and validation of principle. Magn Reson Med. 2001; 46(2):282–291. [PubMed: 11477631]
25. Liu P, Xu F, Lu H. Test-retest reproducibility of a rapid method to measure brain oxygen metabolism. Magn Reson Med. 2013; 69(3):675–681. [PubMed: 22517498]
26. Weber, EC.; Vilensky, JA.; Carmichael, SW. Netter's Concise Radiologic Anatomy. Elsevier Health Sciences; Philadelphia, PA, USA: 2009. Head and Neck.
27. Xu F, Ge Y, Lu H. Noninvasive quantification of whole-brain cerebral metabolic rate of oxygen (CMRO2) by MRI. Magn Reson Med. 2009; 62(1):141–148. [PubMed: 19353674]

28. Fedorov A, Beichel R, Kalpathy-Cramer J, Finet J, Fillion-Robin JC, Pujol S, Bauer C, Jennings D, Fennessy F, Sonka M, Buatti J, Aylward S, Miller JV, Pieper S, Kikinis R. 3D Slicer as an image computing platform for the Quantitative Imaging Network. Magnetic resonance imaging. 2012; 30(9):1323–1341. [PubMed: 22770690]
29. Herscovitch P, Raichle ME. What is the correct value for the brain--blood partition coefficient for water? Journal of cerebral blood flow and metabolism: official journal of the International Society of Cerebral Blood Flow and Metabolism. 1985; 5(1):65–69. [PubMed: 3871783]
30. Liu, P.; Dimitrov, I.; Andrews, T.; Crane, D.; Dariotis, J.; Desmond, J.; Dumas, J.; Gilbert, G.; Kumar, A.; Leroux, J.; MacIntosh, B.; Yang, S.; Xiao, G.; Lu, H. Multi-site evaluations of a TRUST MRI technique to measure brain oxygenation. Salt Lake City, USA: 2013. p. 715
31. Lu H, Xu F, Rodrigue KM, Kennedy KM, Cheng Y, Flicker B, Hebrank AC, Uh J, Park DC. Alterations in cerebral metabolic rate and blood supply across the adult lifespan. Cereb Cortex. 2011; 21(6):1426–1434. [PubMed: 21051551]
32. Altman DI, Perlman JM, Volpe JJ, Powers WJ. Cerebral oxygen metabolism in newborns. Pediatrics. 1993; 92(1):99–104. [PubMed: 8516092]
33. Cragg BG. The development of synapses in the visual system of the cat. The Journal of comparative neurology. 1975; 160(2):147–166. [PubMed: 1112924]
34. Tsumoto T, Suda K, Sato H. Postnatal development of corticotectal neurons in the kitten striate cortex: a quantitative study with the horseradish peroxidase technique. The Journal of comparative neurology. 1983; 219(1):88–99. [PubMed: 6619335]
35. Changeux JP, Danchin A. Selective stabilisation of developing synapses as a mechanism for the specification of neuronal networks. Nature. 1976; 264(5588):705–712. [PubMed: 189195]
36. Cowan WM, Fawcett JW, O'Leary DD, Stanfield BB. Regressive events in neurogenesis. Science. 1984; 225(4668):1258–1265. [PubMed: 6474175]
37. Rao, MS.; Jacobson, M. Developmental neurobiology. Plenum; New York: 2005.
38. Attwell D, Laughlin SB. An energy budget for signaling in the grey matter of the brain. Journal of cerebral blood flow and metabolism: official journal of the International Society of Cerebral Blood Flow and Metabolism. 2001; 21(10):1133–1145. [PubMed: 11598490]
39. Roche-Labarbe N, Wallois F, Ponchel E, Kongolo G, Grebe R. Coupled oxygenation oscillation measured by NIRS and intermittent cerebral activation on EEG in premature infants. Neuroimage. 2007; 36(3):718–727. [PubMed: 17482837]
40. Ohls RK. Core Concepts: The Biology of Hemoglobin. NeoReviews. 2011; 12(1):e29–e38.
41. Dai W, Garcia D, de Bazelaire C, Alsop DC. Continuous flow-driven inversion for arterial spin labeling using pulsed radio frequency and gradient fields. Magn Reson Med. 2008; 60(6):1488–1497. [PubMed: 19025913]
42. Detre JA, Alsop DC. Perfusion magnetic resonance imaging with continuous arterial spin labeling: methods and clinical applications in the central nervous system. Eur J Radiol. 1999; 30(2):115–124. [PubMed: 10401592]
43. Wong EC. Vessel-encoded arterial spin-labeling using pseudocontinuous tagging. Magn Reson Med. 2007; 58(6):1086–1091. [PubMed: 17969084]
44. Golay X, Hendrikse J, Lim TC. Perfusion imaging using arterial spin labeling. Topics in magnetic resonance imaging: TMRI. 2004; 15(1):10–27. [PubMed: 15057170]

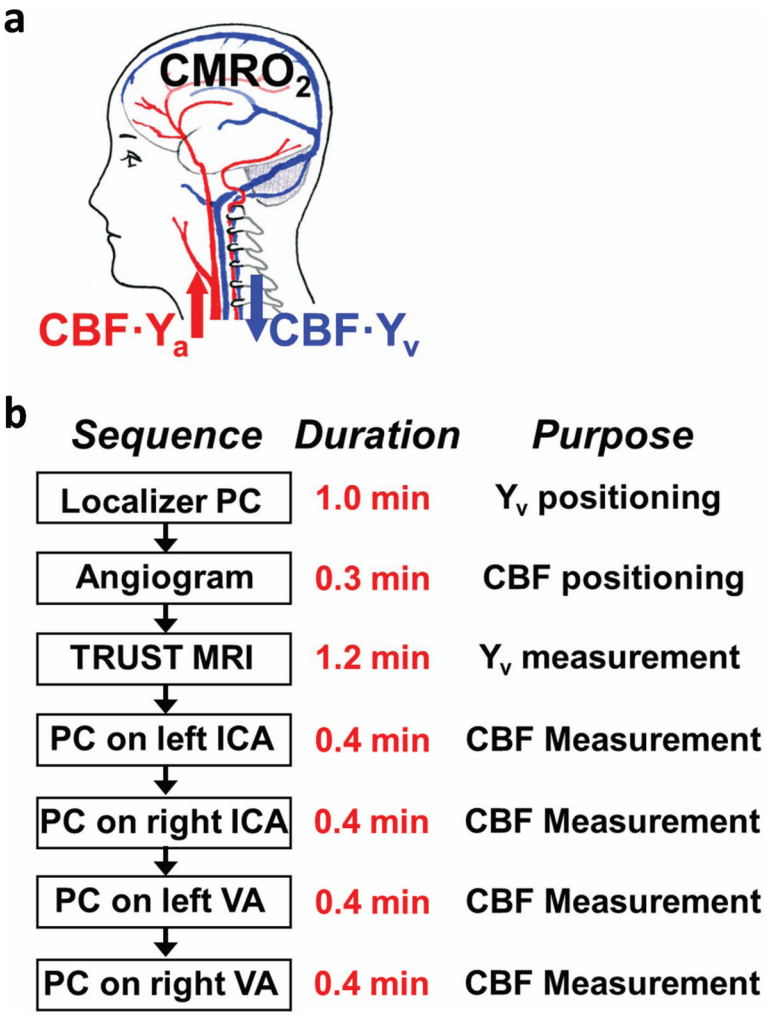

Figure 1.
Framework of $CMRO_2$ measurement using MRI. (a) Illustration of the relationship among different physiologic parameters associated with oxygen demand and supply of the brain. (b) Proposed MRI procedure for a complete $CMRO_2$ dataset in neonates.

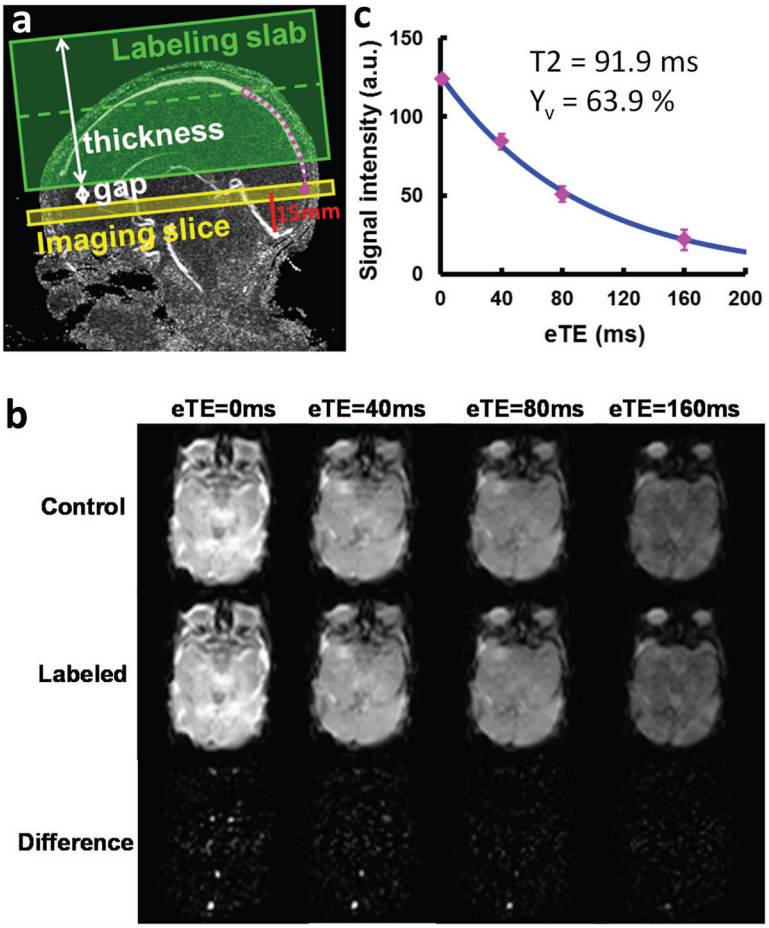

Figure 2.

Measurement of venous oxygenation (Y_v) using T_2-Relaxation-Under-Spin-Tagging (TRUST) MRI. (a) Imaging slice (yellow) and labeling slab (green) of the TRUST MRI scan illustrated on the velocity map of superior sagittal sinus (SSS). The imaging slice was positioned to be parallel to anterior-commissure posterior-commissure line with a distance of 15 mm from the sinus confluence. The labeling thickness and gap were determined by an automatic algorithm based on identifying the location of the blood (open purple circle) at 1022 ms prior to reaching the imaging slice (filled purple circle). (b) MR images under control (top row) and labeled (middle row) conditions. Each type of image is acquired at four different T_2-weightings, denoted by the effective echo time (eTE). The bottom row is the difference image, i.e. Control-Labeled. (c) Monoexponential fitting of the signal intensity in SSS as a function of eTE yields the CPMG T_2 of the venous blood, which is then converted to Y_v via a calibration plot. Error bar indicates standard error of the eTE measurements. The standard error of this Y_v estimation was 3.3%.

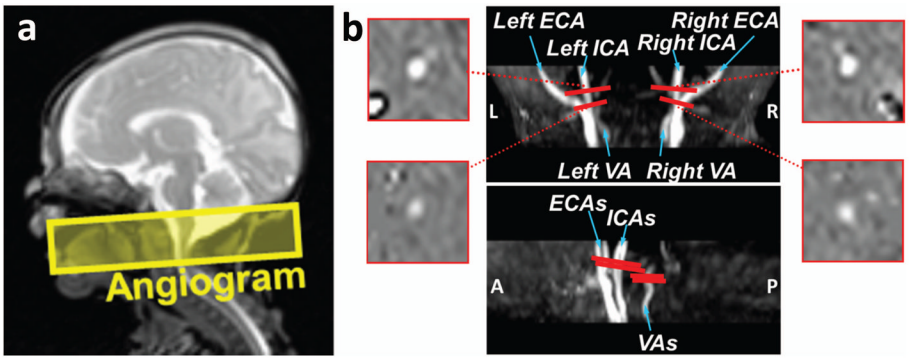

Figure 3.

Measurement of cerebral blood flow (CBF) using Phase-Contrast (PC) MRI. (a) Slice position of the 3D angiogram scan that was used to visualize the feeding arteries. (b) Results of the angiogram scan with slice positions of the PC MRI scans. Center: coronal and sagittal maximum-intensity-projection (MIP) views of the angiogram shown on the scanner (See Supplementary Figure S1 for the post-processed MIP images of ICAs and VAs separately). Four PC MRI scans (red bars) are positioned perpendicular to the respective feeding arteries based on the MIP image of the angiogram. The corresponding phase images of the target arteries from the PC MRI scans are shown on the two sides.

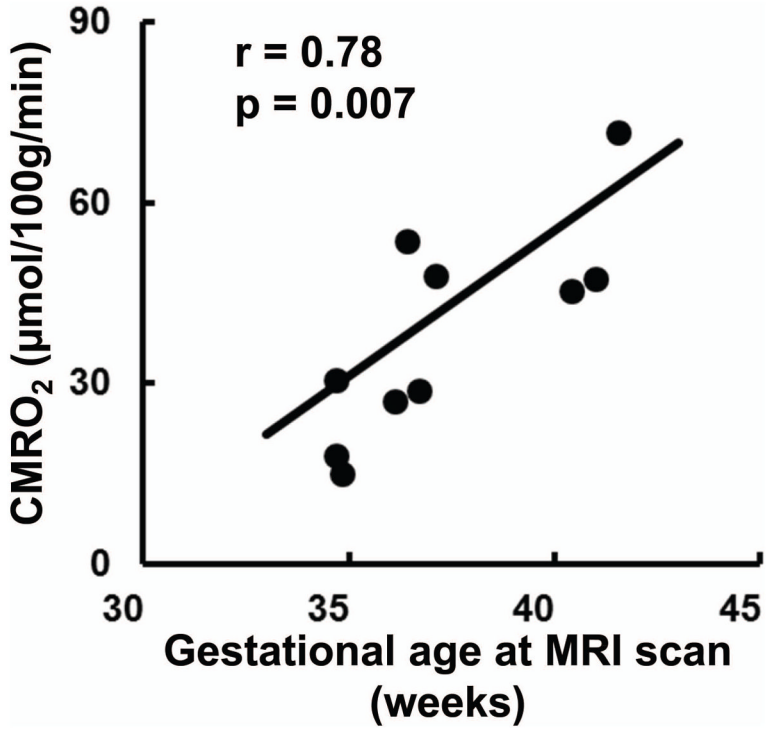

Figure 4.
Correlation between measured $CMRO_2$ and gestational age at scan in 10 neonates (r = 0.78, p = 0.007). Each symbol represents data from one subject. The curve indicates the linear trend line.

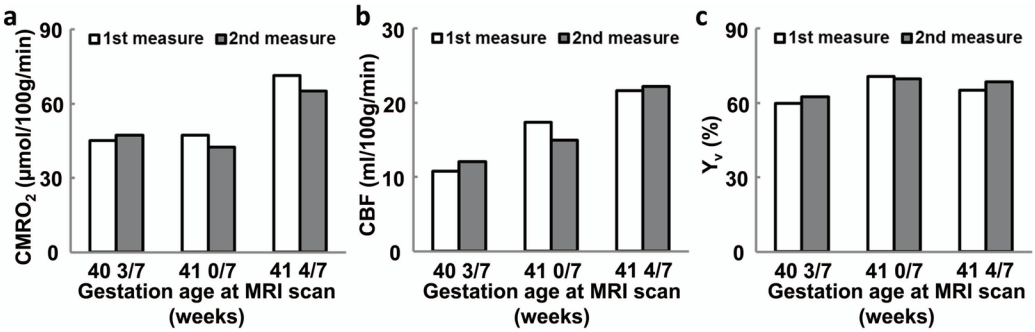

Figure 5.

Test-retest reliability of the experimental measures of (a) $CMRO_2$, (b) Y_v, and (c) CBF in three neonates. Data from each subject are plotted individually with their age specified.

Table 1

Comparison of the $CMRO_2$ obtained from this study with previous reports.

Study	Method	Number of subjects	Gestational age (weeks)	Subject condition	Y_v (%)	CBF (ml/100g/min)	$CMRO_2$ (μmol/100g/min)
Skov et al, 1993 (9)	NIRS	32	26 – 39	Asphyxiated; RDS	53.44±15.36 (preterm) 67.30±9.38 (term)	12.6±6.4 (preterm) 26.5±17.9 (term)	44.7±17.9 (preterm) 62.6±35.8 (term)
Altman et al, 1993 (32)	PET	11	26 – 41	HIE and other conditions	-	21.6±21.0	21.4±16.4
Yoxall and weindling, 1998 (10)	NIRS	20	24 – 41	Seizure and other conditions	64.6 (76.1 – 46.8)	9.3 (4.5 – 28.3)	23.1 (8.6 – 78.5)
Elwell et all, 2005 (8)	NIRS	9	23 – 37	Ventilatory support	-	-	45.9±12.3
This study	MRI	12	35 – 42	Healthy	62.6±8.3	13.4±4.2	38.3±17.7

NIRS - near infrared spectroscopy.

PET - positron emission tomography.

MRI - magnetic resonance imaging.

RDS – Respiratory distress syndrome

HIE – Hypoxic-ischemic encephalopathy